30 Mar 2001, 4:30 pm - 6:30 pm

Foundation-Soil-Inclusion Interaction Modelling for Rion-Antirion Bridge Seismic Analysis

Dan Yang
Buckland & Taylor Ltd., Canada

Ricardo Dobry
Rensselaer Polytechnic Institute, Troy, NY

Ralph B. Peck
Albuquerque, NM

FOUNDATION-SOIL-INCLUSION INTERACTION MODELING FOR RION-ANTIRION BRIDGE SEISMIC ANALYSIS

Dan Yang
Buckland & Taylor Ltd.
1591 Bowser Avenue
North Vancouver, BC V7P 2Y4, Canada

Ricardo Dobry
Dept. of Civil Engineering
Rensselaer Polytechnic Institute
Troy, NY 12180-3590

Ralph B. Peck
1101 Warm Sands Drive, SE
Albuquerque
New Mexico 87123

ABSTRACT

The Rion-Antirion Bridge in Greece will span a total length of 3521m, which includes a five span cable-stayed bridge 2252m in length and two approach viaducts. Upon completion in 2004, the bridge will be the longest cable-stayed bridge in the world. The main factors affecting the foundation design involve high seismicity, poor in-situ soil conditions, deep sea water (65m) and high ship impact force. These factors called for an innovative foundation design for each of the 90m diameter piers by the foundation designer, Geodynamique et Structure (GDS) from France. The proposed design consists of vertical open-ended steel cylinders (called "inclusions"), 25 to 30m long and 2m in diameter, which will reinforce the in-situ soils. The inclusions are to be spaced at 7 to 8m beneath each pier footing supporting a 230m tall pier and pylon structure. These inclusions are not connected structurally to the footing. Beneath each footing is to be placed a layer of gravel in which the inclusion heads are to be embedded. The interface between the pier base and gravel is to serve as a sliding shear fuse under extreme earthquake loading, involving a base isolation concept. This design was checked independently by the Checker - Buckland & Taylor Ltd. (B&T), using nonlinear finite element analyses of the foundation and soil subjected to equivalent seismic or ship impact loading consisting of a horizontal monotonic or cyclic force acting at a representative height (lever arm) above the seabed. The failure mechanisms observed in centrifuge model tests and in field sliding tests of the footing were closely examined and compared with the failure behavior predicted by the finite element soil-structure interaction modeling. The hysteretic damping characteristics of the foundation under horizontal cyclic loading obtained from the above analyses were used in the dynamic global bridge seismic analysis. The Checker's independent analyses confirmed the viability of the proposed design.

INTRODUCTION

The Bridge and The Site Seismicity

The Rion-Antirion Bridge will link southern Greece near the town of Patras (Patrai) to central Greece across the western tip of the Gulf of Corinth (Fig. 1). This link consists of a cable-stayed bridge with five spans, three central spans of 560m each and two flanking spans of 286m. During the design, the engineers faced the following design challenges: 1) high seismicity and tectonic movements related to a fault system in the area of the bridge site; 2) deep soil strata characterized by interbedded lenticular soft clay, silt and sand in excess of 500m; 3) sea water depths up to 65m; and 4) large horizontal force and overturning moment due to earthquake, ship impact and wind. In terms of magnitude of loading, eccentric loads induced by the design earthquake and the design ship impact are much greater than those induced by wind. To alleviate potential damage to the structure due to all the above, each composite steel and concrete main span is designed to be a continuous span with a transverse passive damping (I/D) system at the connection of the deck to the pylon so the bridge can withstand strong motions and large tectonic movements up to 2m in any direction. The strong motions are characterized by a peak ground acceleration of 0.48g at seabed level and by the surface design spectrum shown in Fig. 2 (KME, 1992).

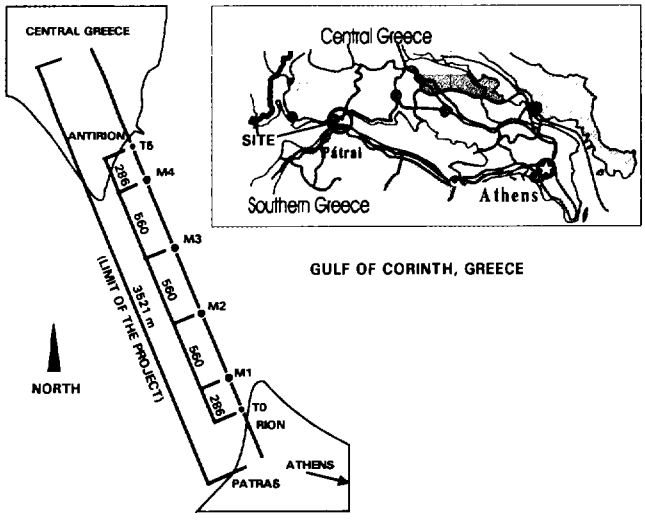

Fig. 1. Rion-Antirion Bridge location plan

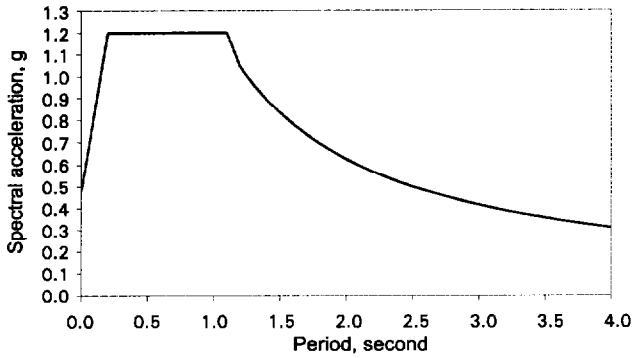

Fig. 2. Design response spectrum (KME, 1992)

Site Investigation and Soil Profile

The subsurface exploration was carried out by various offshore exploratory methods with depths up to 100m (Geodynamique et Structure, 1997), principally by penetration tests using piezocone and seismic cone, supplemented by direct sampling and testing and several other forms of in-situ tests. Generalized profiles as interpreted from the site investigations are shown in Fig. 3. No bedrock was encountered during the offshore drilling. The bedrock is believed to be at depths more than 500m below the seabed. The undrained shear strength of the in-situ soils was primarily inferred from the cone data. Figure 4 shows the inferred undrained shear strength from a set of cone data (PCPT), the design lower and upper bound strengths and several measurements of laboratory undrained shear strength. The soil strata are mostly normally consolidated. For the sandy layers where a liquefaction assessment showed high potential for liquefaction under the design earthquake, the lower bound shear strengths correspond to their estimated post-liquefaction residual strengths. The upper bound shear strengths were limited to the apparent drained shear strengths for those sandy layers where the drained shear strengths were lower than the inferred shear strengths from the cone data.

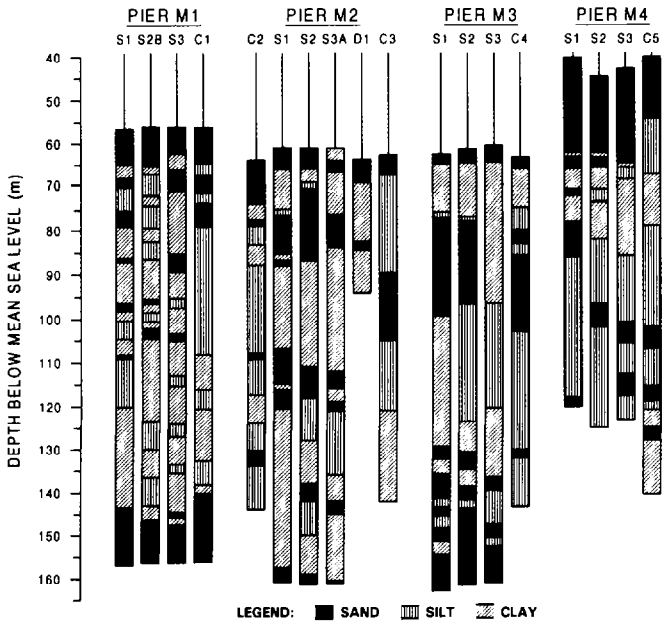

Fig. 3. Generalized soil profiles at four main piers

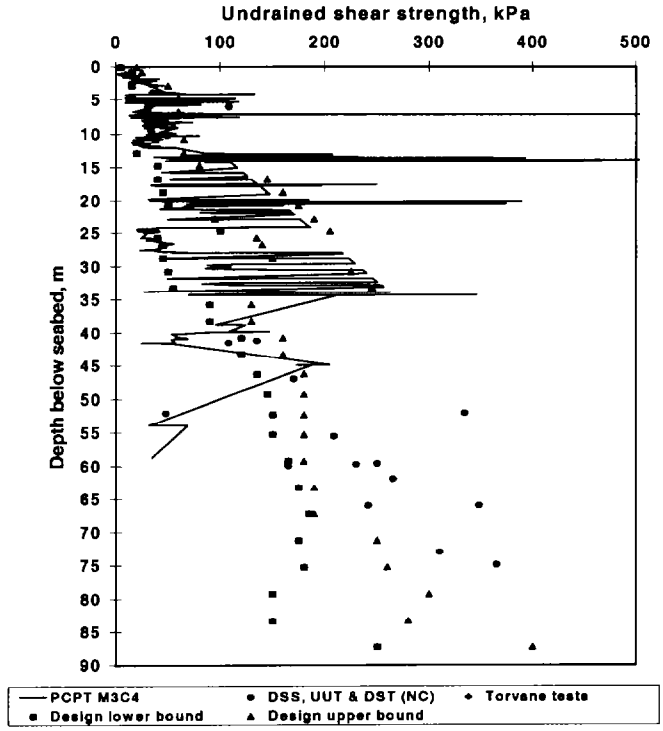

Fig. 4. Undrained shear strengths at pier M3

Foundation Design

The high seismicity and large tectonic movements at the bridge site require the bridge to have flexibility as well as resilience in both pier foundations and pylon structures. In the pylon structures, a passive isolation/dissipation (I/D) system is provided between the deck and the pylon base at main piers M1 to M4. Because the deep soft marine soil strata preclude any deep foundation reaching bedrock, the foundation designer proposed an innovative design involving a base isolation concept. The foundation configuration consists of large diameter (90m) pier bases, resting on a gravel ballast layer placed on top of a volume of uniformly reinforced soil media using steel inclusions extended for several additional rows in a ring outside the footing (Fig. 5). The pier bases are to be constructed in a dry dock, then in a wet dock on the Antirion side, and are to be floated to the final position and set down by permanent water ballast. A total number of about 270 hollow steel inclusions of 25 to 30m length and 2m in diameter with 20mm wall thickness, are to be driven into the soil at a spacing of 7 to 8m. The inclusion heads are embedded in the gravel, at 0.75m below the pier footing. While the steel inclusions will significantly increase the shear strength of the in-situ soil and thus the vertical static bearing capacity, the fact that the inclusions are not connected structurally to the footing means that the inertial shear force generated by the superstructure during strong shaking is limited by sliding friction at the footing-gravel interface. The soil reinforcement scheme used in the design employs principles similar to those of soil nailing (Pecker and Teyssandier, 1998). However, use of base isolation, which is well established for seismic design of buildings, is new in long span bridge foundation design.

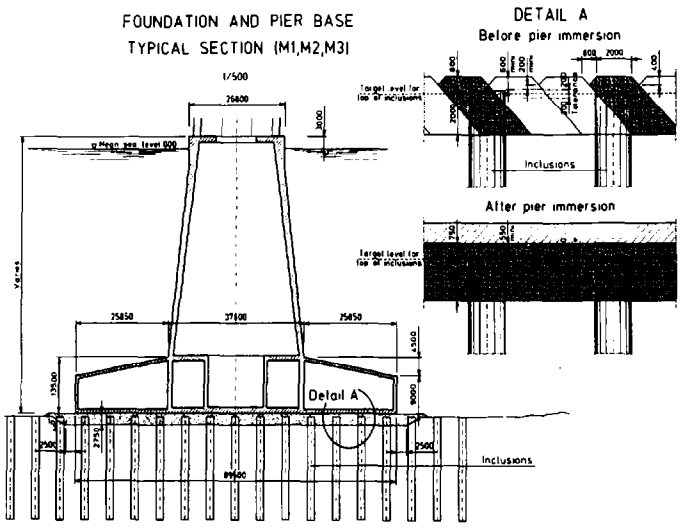

Fig. 5. A typical section of the foundation design

Analyses

In order to confirm the base isolation design concept and to provide the foundation response characteristics for dynamic global bridge seismic soil-structure interaction modeling, the Checker conducted a comprehensive study to determine:

- the static vertical as well as the pseudo-static horizontal load and displacement capacities of the bridge foundation under various loading conditions placed upon it by the design earthquake and ship impact loads;
- the hysteretic behavior of the foundation under cyclic lateral loading conditions, including internal hysteretic damping dissipation characteristics and the validity of the Masing criterion for use in the Checker's independent dynamic global bridge seismic analysis; and
- sensitivity of the design foundation capacity to variations in the soil parameters and modeling details.

The principal approach used to conduct the above analyses was 2D and 3D nonlinear finite element (FE) modeling, which modeled explicitly the interactions between footing, soil media and steel inclusions. The software used was the nonlinear finite element package ABAQUS. Different overturning moments and load eccentricities were achieved by placing a horizontal load, F, at a distance (lever arm) above seabed (Fig. 6). The numerical models predicted different failure mechanisms for the various horizontal load eccentricities, and these mechanisms were closely examined and compared with those observed in the centrifuge model tests and field sliding tests of the footing conducted at the bridge site by the foundation designer and the Contractor.

The foundation designer had carried out extensive analytical and numerical studies, including limit equilibrium analyses based on the yield design theory (Salencon and Pecker, 1995) and 2D nonlinear finite element analyses (Geodynamique et Structure, 1999a). The results of these studies were compared with the numerical results obtained by the Checker.

SOIL-STRUCTURE INTERACTION ANALYSES

2D and 3D Numerical Models of the Pier Foundation

To analyze the proposed foundation configuration, numerical models were created in 2D and 3D, respectively. The 2D model, shown in Fig. 6, was based on an equivalent rectangular footing of 78m by 82m, which has the same area and moment of inertia as the 90m diameter circular pier base. The pier base was modeled as a steel frame using beam elements supported by a concrete footing modeled using solid elements. A normal pressure of 117kPa was applied to the footing. The gravel ballast layer was modeled as a fully drained material with a friction angle of 40°. The pier footing-gravel layer interface was modeled as contact surfaces with an interface friction angle of 35°. These contact surfaces allow simulation of footing slippage at the interface due to sliding failure, and of footing uplift due to large footing rotation. Twelve in-situ soil layers were modeled as undrained materials with the lower bound undrained shear strengths shown in Fig. 4. The inclusions were modeled as elastic beam elements, with contact surfaces used at both sides of each inclusion to allow for potential slippage of these inclusion-soil interfaces. An undrained shear limit of 100kPa was assigned to the interfaces. Nonlinear soil springs were used at the inclusion tips to simulate the proper tip bearing capacity for the open-ended steel cylinders. As the onshore inclusion driveability test indicated very little soil plugging (IHC, 1998), the open-ended tip bearing capacity was used as the yield force of these nonlinear soil springs.

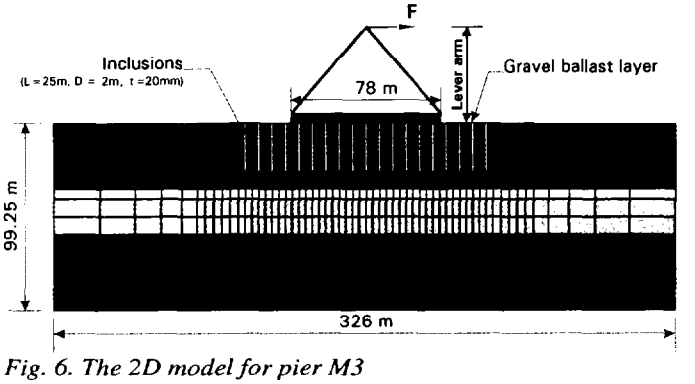

Fig. 6. The 2D model for pier M3

The 3D model is shown in Fig. 7. The modeling details used were the same as those used in the 2D model, except that the contact surfaces along individual inclusions were removed. A calculation of the global energy dissipated in the system during a loading-unloading-reloading cycle of the horizontal force shown in Fig. 6 (Dobry et al., 1999) had indicated that these contact surfaces contributed less than 5% of the total energy dissipated. Most of the energy was dissipated at the pier base-gravel interface and the upper two layers of soil. Therefore, the removal of these contact surfaces along inclusions did not result in a significant change in energy balancing. Instead, it improved convergence speed significantly. In the 3D model, the vertical model dimension of the soil media was extended to accommodate a much larger stress influence zone, so as to

eliminate the numerical model boundary effect when the model is subject to a vertical monotonic loading condition. Only one half of the 3D foundation configuration was modeled to save computational time.

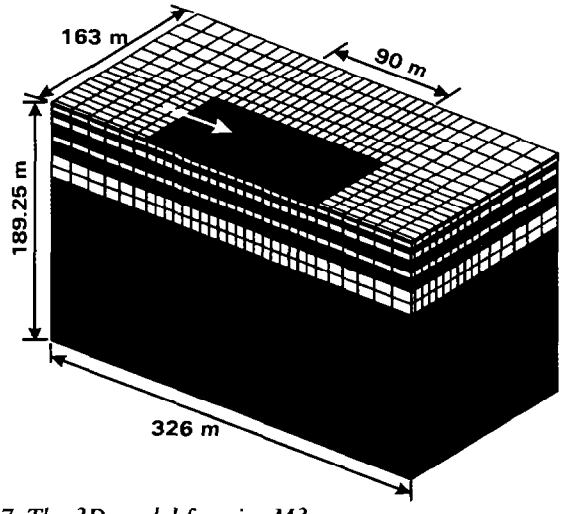

Fig. 7. The 3D model for pier M3

Elastic-Plastic Soil Material Models

Two elastic-plastic soil material models were selected for each soil layer on the basis of the laboratory triaxial test results as illustrated in Fig. 8. The first model was elastic-perfectly plastic with an elastic stiffness equal to G_{50} for each soil layer. G_{50} is defined as the tangent slope of a stress-strain curve at a stress equal to 50% of its ultimate strength. The second model, which matched better the triaxial data, was a "piecewise-linear" elastic-plastic model with kinematic hardening.

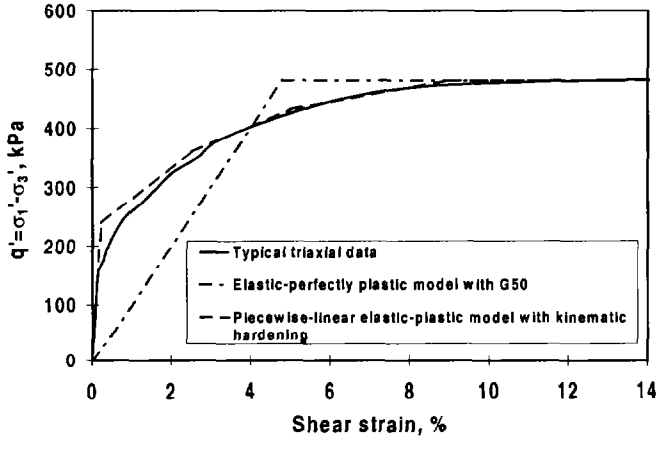

Fig. 8. Two typical soil material models used for a soil layer

When used for the drained gravel ballast layer, the two models were governed by the Mohr-Coulomb yield criterion and non-associated flow rules. When used for the undrained in-situ soil layers, the two models were governed by the Von Mises yield criterion and associated flow rules. The predicted failure loads for the foundation system using either model should be similar, because both soil models have the same ultimate shear strength at a given soil element. However, it is anticipated that the predicted global hysteretic damping ratios of the foundation will be different, because the energy dissipation characteristics inherent to the two soil models are different. A predicted failure load in this study is defined as the load at which a large failure displacement has occurred and the last load increment is less than 2% of the total load applied on the footing.

Failure Mechanisms Predicted by Numerical Modeling

Three distinctive failure mechanisms were predicted from the soil-structure interaction modeling: a sliding mode, a combined sliding/rotational mode, and a rotational mode.

Sliding Failure Mode. This failure mode featuring a horizontal sliding with little footing rotation occurred at low horizontal load eccentricities with lever arms less than about 25m. This failure mode predicted by the numerical models was confirmed by field sliding tests with a low horizontal load eccentricity equivalent to a full-scale lever arm of 13.2m (Koinopraxia Gefyra, 2000).

Combined Sliding/Rotational Failure Mode. This failure mode occurred at lever arms between 25m and 45m. Figures 9 and 10 illustrate the displacement vectors and the deformed mesh, respectively, of the gravel ballast layer and nine layers of in-situ soil associated with this failure mode. Figure 10 also shows the plastic strain distribution in the soil media at failure. The predicted inclusion deflections are shown in Fig. 11.

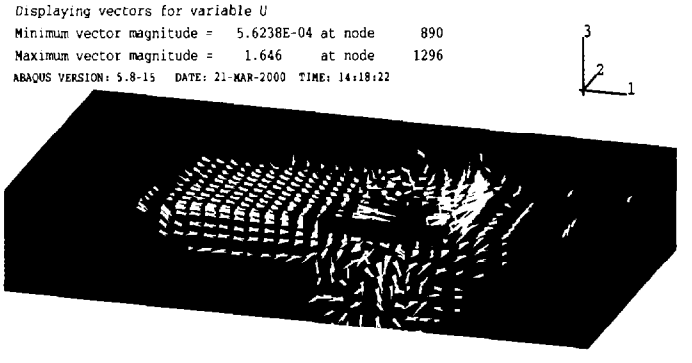

Fig. 9. Displacement vector in soil at failure (lever arm=30m)

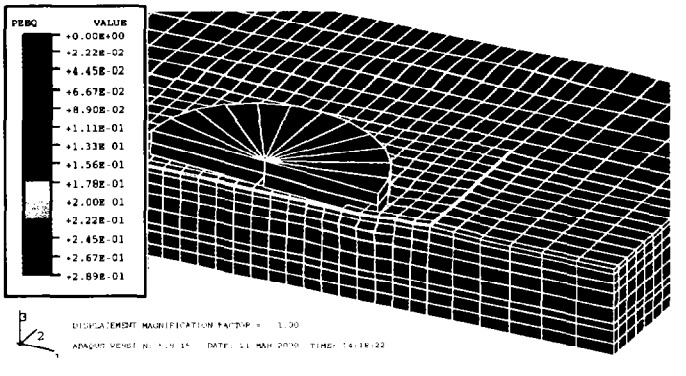

Fig. 10. Deformed mesh and plastic strain (see legend) at failure by the 3D model (lever arm=30m)

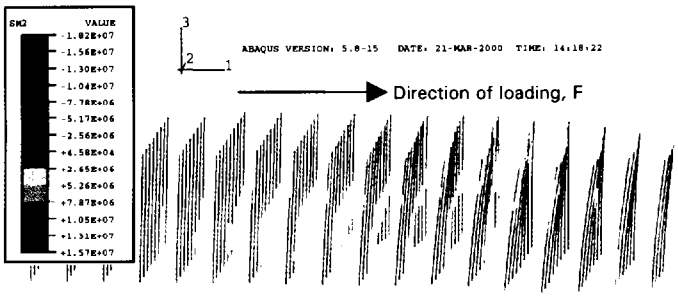

Fig. 11. Deflected shapes and bending moments (N-m, see legend) of inclusions at failure by the 3D model (lever arm=30m)

Small-scale models (1:300 of the full-scale foundation configuration) under similar eccentric lateral loading were also tested in centrifuges. A series of centrifuge model tests under lateral loading conditions was conducted at French research institutes Centre D'Etudes Scientifiques et Techniques D'Aquitaine (CESTA) and Laboratoire Central des Ponts et Chaussees (LCPC). The tests were designed to validate the new design concept by providing information on the ultimate lateral bearing capacities of the foundation and its failure behavior. The interpretations of the test results are presented in Geodynamique et Structure (1999b and 1998) and LCPC (1998). The soils used in the centrifuge tests were retrieved from the bridge site. They were prepared by a homogenization procedure in which a layer of sand was laid on top of the homogenized clay with another drainage layer of sand at the bottom. The consolidation phases included an on-bench (1g) hydraulic gradient consolidation phase followed by an in-flight (centrifugal) consolidation phase. Figure 12 shows the footing deformation after failure for a centrifuge test with a full-scale equivalent lever arm of 30m. The failure mode obtained from this centrifuge test was of special interest for comparing with the failure mode predicted by the numerical model. The centrifuge test failure behavior shows two distinctive features: one is digging of the front toe into the soils and the other is uplift of the footing tension side. Both features are well modeled by the numerical model under similar loading as shown in Figs. 9 and 10. The predicted and observed inclusion deflections also match each other as shown in Figs. 11 and 13. The bending moments calculated for the inclusions shown in Fig. 11 indicate that all inclusions remain elastic at failure (the steel inclusion ultimate plastic moment = 2.9E7 N-m).

Rotational Failure Mode. This failure mode occurred at lever arms higher than about 45m. Under such high eccentricity, the foundation became unstable with increasing monotonic loading. Soil yielding occurred only in a localized area directly under the front toe of the footing. The remaining soil media experienced much smaller shear stresses that were well below their shear strengths. The stress concentration predicted by the numerical model for this failure mode is illustrated by the contact pressure distribution at the pier base-ballast layer interface shown in Fig. 14. In this figure, the red gridlines outline the contact surface on the outer surface of the pier base, whereas the white gridlines outline the contact surface on the top surface of the ballast layer.

Footing deformation after failure

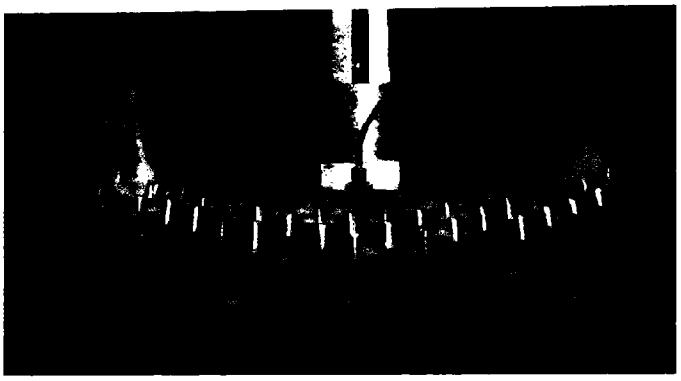

Fig. 12. Failure behavior from a centrifuge test (full-scale equivalent lever arm=30m)

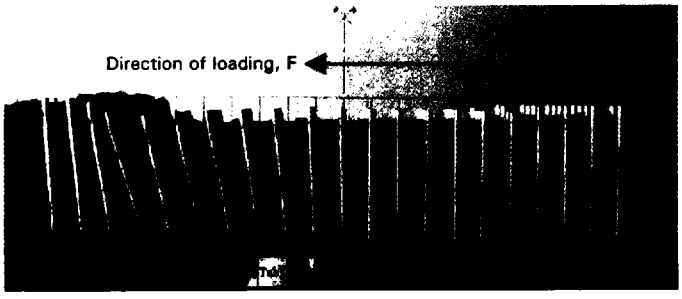

Fig. 13. Deflected shapes of inclusions in a centrifuge model (full-scale equivalent lever arm=30m)

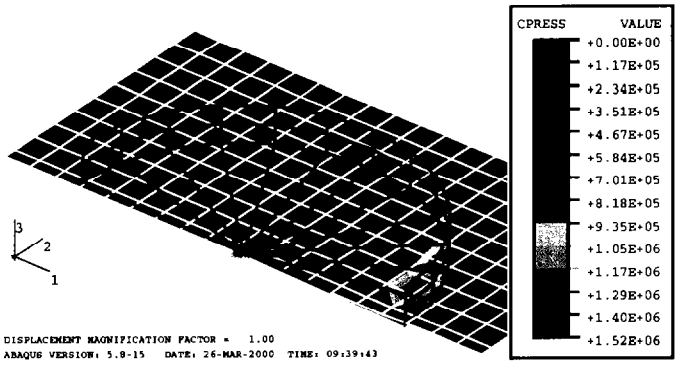

Fig. 14. Contact pressure (N/m^2, see legend) at failure in two contact surfaces by the 3D model (lever arm=50m)

Effects of Steel Inclusions on the Failure Behavior

The steel inclusions were designed to provide additional shear resistance to the soft marine sediments, thus acting as soil-reinforcing elements. The numerical model analyses confirmed this concept. Without the inclusions, the numerical model under monotonic horizontal loading showed a global failure in the soil media with a continuous failure surface and very large plastic deformations (Fig. 15). In contrast, the numerical model with the inclusions always showed a local failure directly under the toe of the footing and at the tips of several inclusions near the toe, with much smaller plastic deformations (Fig. 16) and a higher failure load.

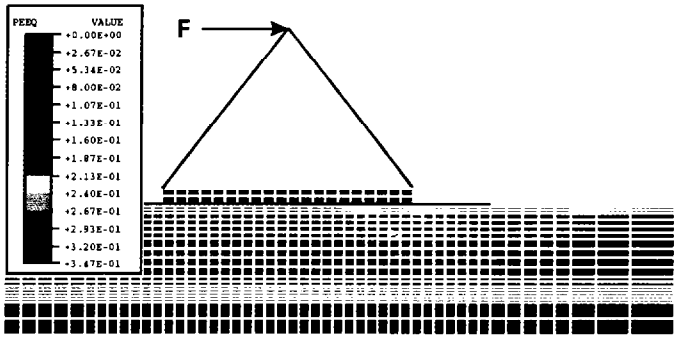

Fig. 15. Plastic strain (see legend) distribution without inclusions by the 2D model (lever arm=50m)

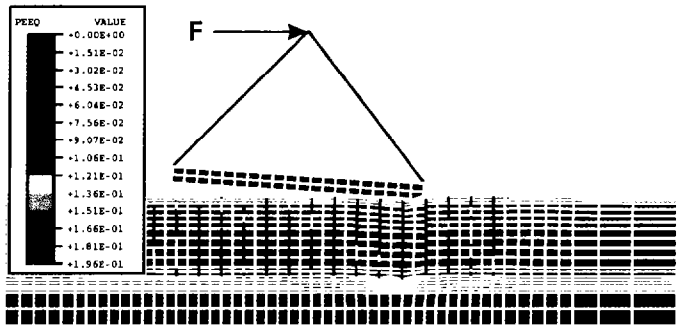

Fig. 16. Plastic strain (see legend) distribution with inclusions by the 2D model (lever arm=50m)

The inclusions also acted as load paths to transfer loads into deeper soil strata near their tips. In a sensitivity study (Yang et al., 1999b), the upper two layers of 8m thick clay in the 3D model were weakened by reducing their shear strengths to 7.5kPa and 15kPa, respectively, i.e. one half of their original values. In both the original and the weakened 3D models, the foundation was loaded vertically. The weakened model showed two stages of yielding. The initial yielding was due to soil plastification in the two weakened clay layers. As the plastic deformations developed, the inclusions became engaged with the pier footing and created new load paths to carry load to the deeper stronger soil strata. The final yielding was caused by soil plastification near the inclusion tips. As compared to the original model, the change in the predicted failure load by the weakened model was small.

Comparison of Designer's and Checker's 2D Results

The comparison of the Checker's 2D modeling results with the foundation designer's results, both for the pier M3 foundation with lower bound soil properties, is shown in Fig. 17, presented as predicted horizontal ultimate failure load versus ultimate overturning moment for various horizontal load lever arms. The foundation designer's analyses were conducted using nonlinear FE package DYNAFLOW. Also shown in Fig. 17 are the results of limit equilibrium analyses based on the yield theory. The foundation ultimate capacities under different lever arms predicted by three independent analyses are reasonably close to each other. In particular, the results of two sets of FE analyses conducted by the Checker and the foundation designer for 30m and 50m lever arms match each other well. The FE predicted foundation failure mechanisms, i.e. sliding, combined sliding/rotational, or rotational failure mechanism are close to each other in corresponding FE runs, and they are confirmed by the field sliding tests and the centrifuge model tests. The horizontal force-displacement curves predicted for the foundation response to monotonic loading by the foundation designer and the Checker also match each other as shown in Fig. 18.

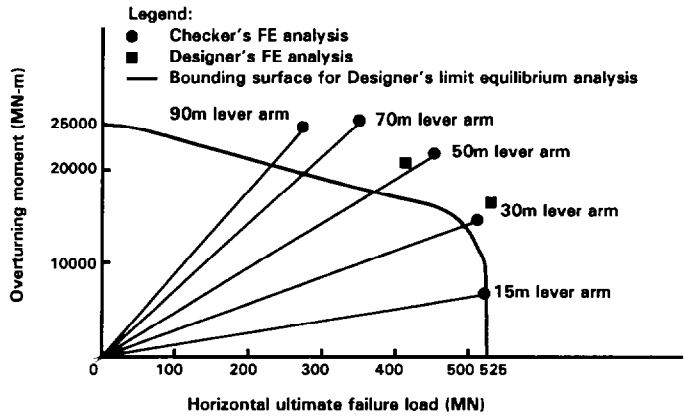

Fig. 17. Comparison of 2D analysis results for pier M3

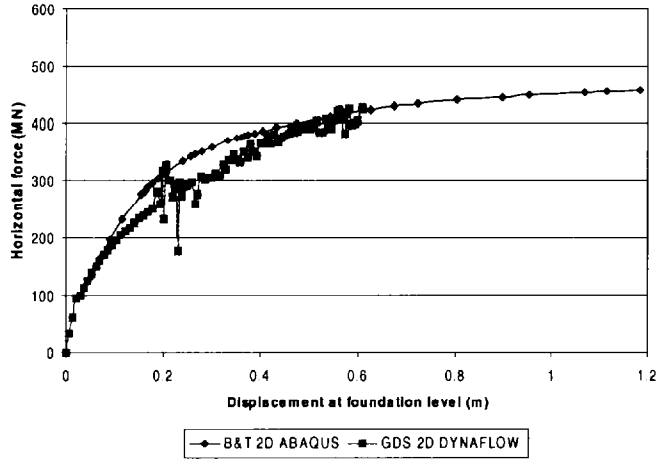

Fig. 18. Comparison of load-displacement curves for pier M3 (lever arm=50m)

Comparison of Checker's 2D and 3D Results and 3D Effects

The horizontal ultimate failure loads predicted for various lever arms were generally greater for the 3D than for the 2D FE models, as shown in Fig. 19. The differences were clearly due to 3D effects. The analyses conducted by the Checker show that the vertical edge around the circular pier base had a significant impact on predicted failure behavior and failure load. This vertical edge surface is part of the 3D contact surfaces (that can be viewed in Fig. 14) specified between the pier base and the ballast layer for potential penetration of the pier base into the ballast layer. In the 3D run of 30m lever arm shown in Fig. 19, a sliding mechanism developed along the horizontal contact surface at the pier base-ballast layer interface, and simultaneously a digging-in mechanism also developed along the vertical contact surface at the pier base vertical edge-ballast layer interface. The sliding mechanism resulted in uniform horizontal soil deformations beneath the footing shown in Fig. 9 and a constant friction shear force equal to $\mu*W$ = 525MN (where μ= friction coefficient at the pier base-ballast layer interface=0.7, and W= total effective weight of the pier=750MN). It was the digging-in mechanism that resulted in the mobilization of passive earth pressure in the soil mass, with a bowl-shaped failure surface developing near the front edge of the pier footing as shown in Fig. 9, thus developed additional lateral bearing capacity. This 3D vertical edge effect revealed by the 3D modeling for the 30m lever arm did not have an impact on the predicted failure load for the 70m lever arm case because the pier toppled with increasing overturning moment before the soil strengths were mobilized. The 3D vertical edge effect had only a moderate impact on the 50m lever arm case.

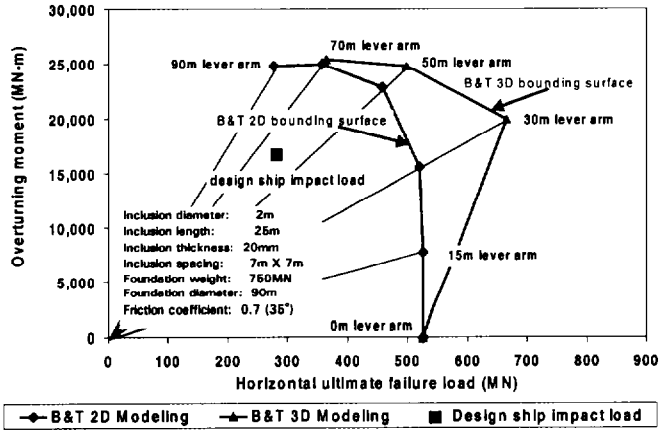

Fig. 19. Comparison of 2D and 3D results for pier M3

The varying safety margins at the different lever arms between the 2D and 3D numerical analyses gave the Checker additional confidence on the load carrying capacities of the pier supporting the pylon and the deck. In particular, the 30m and 50m lever arm cases represent the most significant pseudo-static horizontal load cases. For example, the application points of the ship impact load are located at the mean sea level about 40 to 60m above seabed, varying from pier to pier. The design pseudo-static horizontal ship impact load for the tanker class ships is 280MN and the resulting overturning moment is 16800 MN-m due to the 60m water depth at pier M3, shown as a solid square in Fig. 19. The safety factor according to both the 2D and 3D bounding surfaces in Fig. 19 is considered adequate for this ultimate limit state case.

In the case of a seismic event, the time history analyses show that the majority of the effective heights above seabed of the seismic demands are equivalent to lever arms less than 40m (Fig. 20). When the unfactored seismic demands are plotted against the yield bounding surfaces as shown in Fig. 20, it is clear that most seismic demands did not exceed the 2D bounding surface and none exceeded the 3D bounding surface. A small number of seismic demands located outside the 2D bounding surface may indicate a scenario that the pier undergoes some incipient sliding. However, seismic demands are not sustained loads, and any incipient sliding would only be a transient event. The time history analyses also show that the total permanent deformation due to sliding and inelastic deformation of soil media is less than 0.35m and the total footing rotation is less than 0.003 radians. These are translated to a lateral movement at the top of the pylon in the order of 1.0m (Priestley et al., 1999), which is considered acceptable.

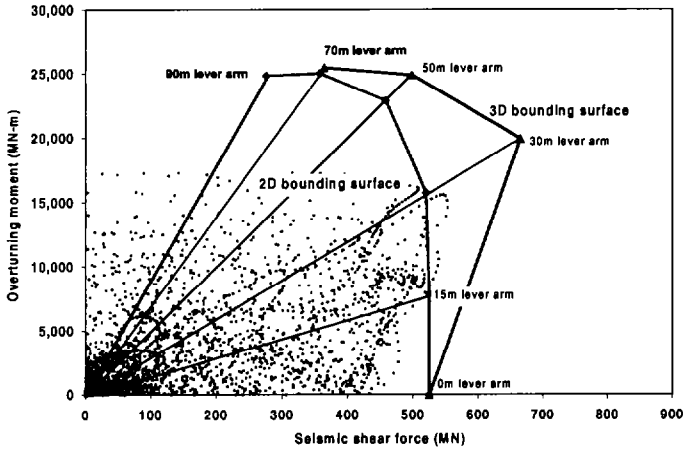

Fig. 20. Seismic demands vs. ultimate yield bounding surfaces

NONLINEAR SOIL SPRINGS FOR SEISMIC ANALYSIS

Hysteretic Damping Behavior and Hysteresis Loops

The internal hysteretic damping dissipation characteristics of the foundation system were obtained based on 2D horizontal loading-unloading-reloading analyses (Yang et al., 1999a). The horizontal cyclic load was applied pseudo-statically to the pier footing with a lever arm of 30m. The validity of the Masing criterion (Kramer, 1996) for use in the global bridge seismic analyses was confirmed by global energy and damping calculations of the 2D FE pseudo-static cyclic analysis results (Dobry et al., 1999).

The internal hysteretic damping dissipation characteristics calculated based on the FE cyclic analyses were a function of the elastic-plastic soil material models used. The two types of

models used are shown in Fig. 8. The resulting horizontal load-displacement hysteresis loops for the foundation system using the two soil models are shown in Figs. 21 and 22. It is apparent that the use of an elastic-perfectly plastic or piecewise-linear elastic-plastic model has a significant impact on the predicted internal hysteretic damping dissipation characteristics of the foundation. The load-displacement hysteresis loops obtained from the elastic-perfectly plastic soil model indicate very small damping at all stages of loading because the soils having the elastic-perfectly plastic behavior do not dissipate energy before yielding. In contrast, the hysteresis loops obtained from the more realistic piecewise-linear elastic-plastic soil model indicate a significantly higher damping, with an equivalent damping ratio of 20% at a horizontal load of 57% of the 700 MN ultimate failure load. When the horizontal load is increased to 86% of the ultimate failure load, the equivalent damping ratio is 26%. Using the backbone curve shown in Fig. 22 obtained from the piecewise-linear soil model, in conjunction with the Masing criterion, the calculated equivalent damping ratios for the above two load levels are 24.6% and 29.8%, respectively. This confirms the validity of using the Masing criterion for the foundation loading-unloading-reloading behavior during the dynamic global bridge seismic analyses.

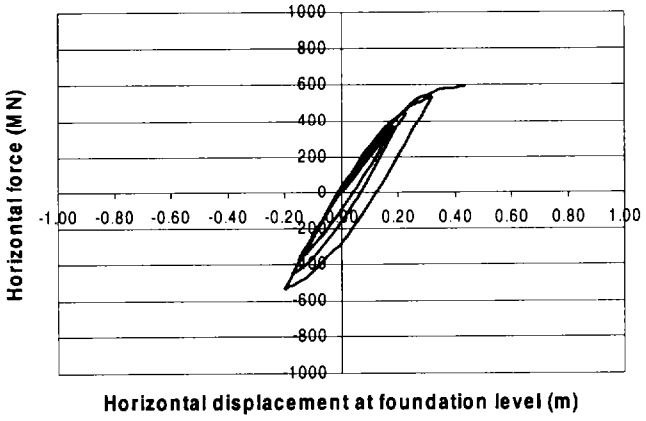

Fig. 21. Hysteretic behavior with an elastic-perfectly plastic soil model with G_{50} (lever arm=30m)

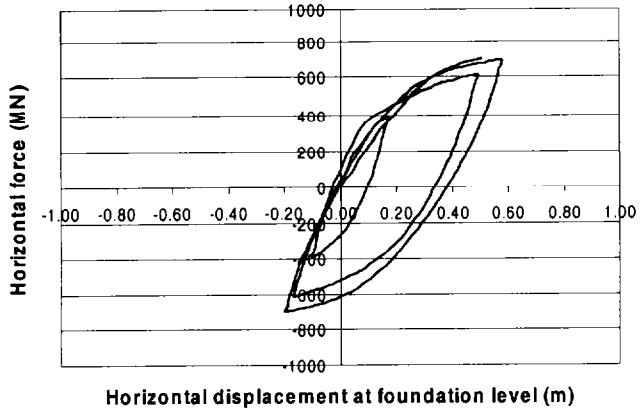

Fig. 22. Hysteretic behavior with a piecewise-linear elastic-plastic soil model with kinematic hardening (lever arm=30m)

Load-Displacement and Moment-Rotation Relationships

The previous section showed that the Masing criterion could be used for modeling the foundation horizontal loading-unloading-reloading behavior in the dynamic global bridge seismic analyses. The corresponding horizontal load-displacement and moment-rotation backbone curves are those obtained from monotonic 2D pseudo-static foundation-soil-inclusion interaction analyses. These lateral load-displacement and moment-rotation relationships were extracted for the four main pier foundations at a lever arm of 30m, as this lever arm is the representative average of the effective lever arms above seabed of the transient seismic demands (Fig. 20). The lateral load-displacement relationship has a sliding fuse cutoff limit of 525MN (=μ*W). The moment-rotation relationship has a rotation cutoff limit of 0.003 radians, associated with a potential footing uplift on the tension side. It was found by the 2D loading-unloading-reloading analyses that the internal damping ratios, in particular the rotational damping ratios, decreased rapidly as footing uplift occurred at rotations greater than 0.003 radians. After tension lift-off occurred at these large rotations, the Masing criterion overestimated the internal damping ratios and hence could no longer be used to model the internal damping dissipation behavior. The time history analyses conducted using lower bound soil properties indicate that the 525MN sliding fuse cutoff limit was rarely exceeded, as illustrated by Fig. 20. The total footing rotation was always less than 0.003 radians which is within the rotation cutoff limit. The total permanent cumulative deformation of the foundation due to the combined effect of sliding and inelastic deformation of the soil media was less than 0.35m.

SETTLEMENT OF THE MAIN PIERS

The foundation designer calculated a consolidation settlement under the vertical static load of about 0.31m for pier M2, expected to experience the largest settlement of the four piers (Geodynamique et Structure, 1999c). On the basis of the laboratory data and the most conservative interpretation, the Checker estimated up to 1m of consolidation settlement. Nevertheless, a settlement of even this magnitude, much of which would occur during construction, would be acceptable.

With respect to tilt, a statistical analysis carried out by the foundation designer using the exploratory data to account for lateral variability of the compressibility, indicates that the magnitude of tilt would be in the order of 0.001 to 0.002 (Geodynamique et Structure, 1999c). Both the foundation designer and the Checker agreed that a field instrumentation program be set up to monitor pier movement. The foundation designer proposed a field instrumentation program, consisting of differential global positioning system (GPS) measurements, in conjunction with conventional vertical angle measurements for both short term and long term monitoring. Should excessive values of tilt be detected during construction, corrections can be made by adjusting the water ballast in the water chambers inside the individual pier bases.

PARAMETRIC STUDY BY FINITE ELEMENT ANALYSIS

Effect of Undrained Shear Slippage Limit at Inclusion-Soil Interfaces

This effect was investigated by the global energy balancing calculation previously discussed in the section of "2D and 3D Numerical Models of the Pier Foundation", and confirmed by a 2D numerical parametric study. In this numerical study, the undrained shear slippage limit at the inclusion-soil interfaces was varied by 100%. The resulting change in the predicted horizontal failure load of the foundation is less than 5%. This study and the global energy balancing calculation provided the basis for the removal of the contact surfaces along the inclusions in the 3D models with anticipation of a negligible influence on predicted failure loads.

Effect of Friction Coefficient at Pier Base-Gravel Ballast Layer Interface

The 2D numerical analyses show that the predicted horizontal failure load for a lever arm of 30m is sensitive to a variation of the friction coefficient from 0.7 to 0.5. The predicted foundation horizontal failure load dropped by 29%. However, the analyses also show that the predicted horizontal failure load for a lever arm of 50m is much less sensitive to the same variation in friction coefficient. In this case, the predicted failure load dropped by less than 5%, because the foundation failure was caused predominantly by footing rotation. This implies that the pier base-gravel ballast layer interface friction characteristics are potentially more significant for the bridge seismic response than for its response to ship impact.

Effect of Random Weak Layers in Soil Media

In general, the predicted failure loads are less sensitive to the undrained shear strength in the soil layer near the inclusion tips, and more sensitive to both the internal friction angle in the gravel ballast layer and the undrained shear strength in the two clay layers just beneath the ballast layer. The sensitivity analyses also show that in the case of random weak layers in the upper two clay layers, the steel inclusions are very effective in bridging the weak layers between the gravel ballast layer and the deeper stronger soil layers, as discussed previously in the section of "Effects of Steel Inclusions on the Failure Behavior".

CONCLUSIONS

The Checker's independent assessment of the Rion-Antirion Bridge foundation design, based on numerical analyses and on examination of centrifuge physical model test evidence and field sliding test results, has reached the following conclusions:

- The foundation configuration for this bridge is capable of meeting the static (vertical) and pseudo-static (horizontal) load and displacement demands placed upon it by this structure and by the project requirements. The base isolation design concept provides flexibility and resilience to the bridge structure.
- The passive isolation/dissipation system to be installed at the connection between the pylon base and the deck, and the reinforced soil-foundation system are two sources of energy dissipation that the bridge structure relies on in the event of the design earthquake. From the Checker's independent study, the foundation internal hysteretic damping amounts to a large portion of the total available damping. The use of the Masing criterion in the dynamic global bridge seismic analysis model is valid.
- The parametric study shows that the friction coefficient is a significant factor that affects the foundation sliding behavior for horizontal loading conditions with lever arms less than 30m. The parametric study also shows that the steel inclusions are effective soil-reinforcing elements, that significantly increase the shear resistance in the soil media and bridge the weak in-situ layers at the shallow depths between the gravel ballast layer and the deeper stronger soil strata.
- Field instrumentation to measure pier settlement and tilting is required for any unforeseeable events that may occur during pier base set-down and superstructure erection. The Checker has accepted the monitoring methods proposed by the foundation designer as economically viable and reasonably accurate approaches.

ACKNOWLEDGEMENTS

The writers wish to thank Mr. Jean-Paul Teyssandier of Gefyra S.A. (the Concessionaire) for permission to publish this paper and his coordination during this on-going project, and to thank Dr. Panayiotis Papanikolas of Koinopraxia Gefyra (the Contractor) and Dr. Alain Pecker of Geodynamique et Structure (the foundation designer) for providing their test and analysis data and their valuable comments. The writers also wish to thank Dr. Peter Taylor and Dr. Vincent Latendresse of Buckland & Taylor Ltd., and Dr. Blair Gohl of Pacific Geodynamics Inc. for their technical assistance and other special contributions to the work discussed in this paper. SEQAD Consulting Engineers, Buckland & Taylor's seismic specialist consultant on this project, conducted the dynamic global bridge seismic analyses.

REFERENCES

Dobry, R., M. Zeghal and G. Mavroeidis [1999]. "Global energy and damping calculations for unloading-reloading of the foundation." Report No. B&T/003/Rev. 0, April 1999.

Geodynamique et Structure [1997]. "Soil investigation at pier

M1, M2, M3 & M4." Report Nos. GDS/00030/0, GDS/00031/0, GDS/00032/0 & GDS/00033/0, July 1997.

Geodynamique et Structure [1998]. "Interpretation of the cyclic centrifuge tests." Report No. GDS/00062/0, Dec. 1998.

Geodynamique et Structure [1999a]. "Updated non-linear load-displacement curves for seismic analyses - Pier M3." Report No. GDS/00067/0, Jan. 1999.

Geodynamique et Structure [1999b]. "Interpretation of centrifuge tests No. 1 to 5." Report No. GDS/00044/0, Mar. 1999.

Geodynamique et Structure [1999c]. "Geostatistical analysis of soil data - Comparative analysis of settlement with and without inclusions." Report No. GDS/00072/0, May 1999.

IHC [1998]. "Installation testpile at Rion-Antirion Link." IHC Hydrohammer bv, Report No. H-43356, Dec. 1998.

KME [1992]. "Regulations for design and investigations for the Rion-Antirion Fixed Link." Hellenic Republic, Ministry of Environment Physical Planning & Public Works, Sept. 1992.

Koinopraxia Gefyra [2000]. "Gravel layer / foundation friction test - Test report." Report No. GKM/23002/A, Feb. 2000.

Kramer, S.L. [1996]. "Geotechnical Earthquake Engineering." Prentice-Hall, Englewood Cliffs, New Jersey, 653pp.

Laboratoire Central des Ponts et Chaussees (LCPC) [1998]. "Centrifuge model tests final report." Report No. LCP/10005/0, Vols. 1 to 3, Oct. 1998.

Pecker, A. and J.-P. Teyssandier [1998]. "Seismic design for the foundations of the Rion Antirion Bridge." Proc. Instn Civil Engrs Geotech. Engng, Vol. 131, Jan., pp. 4-11.

Priestley, M.J.N., M. Calvi, F. Seible, J. Patty, E. Hines and J. Shortreed [1999]. "Rion-Antirion Bridge Seismic Analysis." Report No. B&T/103/Rev. 0, SEQAD Consulting Engineers, Inc., San Diego, California, Sept. 1999.

Salencon, J. and A. Pecker [1995]. "Bearing capacity of shallow foundations under inclined and eccentric loads – Part II: Purely cohesive soil without tensile strength." Eur. J. Mech. A/Solids, Vol. 14, No. 3, pp. 377-396.

Yang, D., V. Latendresse, R.B. Peck, R. Dobry, B. Gohl, D. Bazett and P.R. Taylor [1999a]. "Rion-Antirion Bridge 2D analysis checking of the main bridge foundations." Report No. B&T/002/Rev. 1, May 1999.

Yang, D., V. Latendresse, R.B. Peck, R. Dobry, B. Gohl, D. Bazett and P.R. Taylor [1999b]. "Rion-Antirion Bridge 3D analysis for the main bridge foundations." Report No. B&T/004/Rev. 0, May 1999.